Chapter 2
Quarkonium

Quarkonium is the name given to a sub-atomic system composed of a heavy quark Q and anti-quark $\overline{Q}$, bound by the strong interaction. Quarkonia belong to the more general meson (hadrons composed of a quark anti-quark pair) family of sub-atomic particles but they deserve their own sub-classification due to the many unique properties that distinguish them from the other hadrons. The large masses of the charm (c) and bottom (b) quarks compared to the light (u, d, s) quarks, endow heavy quarkonia with properties that differ significantly from those of the light mesons. A quarkonium system containing a charm and anti-charm ($c\bar{c}$) quark pair is known as charmonium, while the system containing a bottom and anti-bottom ($b\bar{b}$) quark pair is known as bottomonium. Charmonium and bottomonium have both been observed in experiments [1]. The large mass of the top quark affords it with a width so large that it decays via the weak interaction on a timescale below that associated with quarkonium formation. To date, quarkonia composed of top anti-top ($t\bar{t}$) quark pairs (an hypothesised system known as toponium) have not been observed experimentally [1].

Charmonium was first observed experimentally in November 1974 with the famous simultaneous discovery of a narrow state decaying to e^+e^- and $\mu^+\mu^-$ by groups at BNL and SLAC [2, 3]. The new state had a mass of around 3.1 GeV and was quickly interpreted as a bound state of a previously unseen heavy quark and its anti-quark, much heavier than the strange quark. The new quark was named the charm (c) quark and the new bound state came to be known as the J/ψ. Only a few years later in 1977, a further narrow state was observed in decays to $\mu^+\mu^-$ by a group at Fermilab, this time at a mass of around 9.5 GeV [4]. This new state was named Υ (now known as $\Upsilon(1S)$) and provided the first evidence for a further heavy quark, the bottom (b) quark. Following the discovery of the J/ψ and $\Upsilon(1S)$ states, many other quarkonium states were discovered, the masses and quantum numbers of which fitted well with theoretical expectations for $Q\bar{Q}$ bound states.

2.1 Quarkonium Spectroscopy

Quarkonium states are typically categorised according to the total spin of the $Q\bar{Q}$ system S, the orbital angular momentum between the $Q\bar{Q}$ pair, L, and the total angular momentum ($\vec{J} = \vec{L} + \vec{S}$) of the system, J. The spectroscpic notation $n^{2S+1}L_J$, where n is the principal quantum number, is often used to label the quarkonium states. The parity P of a $Q\bar{Q}$ system is given by $P = (-1)^{L+1}$ and the charge conjugation parity C is given by $C = (-1)^{L+S}$. Parity and charge conjugation parity are both conserved quantities in the strong and electromagnetic decays of quarkonium states.

The quarkonium states with masses below the threshold for decays to open-flavour hadrons (i.e. containing non-zero flavour quantum numbers) to be kinematically allowed ($m_{D\bar{D}} \approx 3.74$ GeV for charmonium and $m_{B\bar{B}} \approx 10.56$ GeV for bottomonium) are typically narrow states which decay via the electromagnetic and strong interactions to lower mass quarkonium states, light hadrons or charged leptons. Quarkonium states above the relevant open-flavour threshold generally have much larger total decay widths that are dominated by strong decays to open-flavour hadrons. All of the charmonium states expected to exist below the $D\bar{D}$ threshold have been discovered experimentally. The majority of the bottomonium states expected below the $B\bar{B}$ threshold have also been observed with the exception of the $\eta_b(3S)$, $h_b(3P)$ and most of the D-wave bottomonium states [1]. Figures 2.1 and 2.2 show the experimentally observed (and predicted) charmonium and bottomonium states respectively.

Fig. 2.1 The experimentally observed charmonium states. The states labelled X, the nature of which is unknown, are not thought to be conventional charmonium states. Figure from Ref. [1]

Fig. 2.2 The experimentally observed and theoretically expected bottomonium states. *Dashed lines* denote unobserved or unconfirmed states (an unconfirmed experimental candidate for the $\eta_b(2S)$ state has been observed by the Belle experiment [6]). Figure from Ref. [1]

The properties of the experimentally observed quarkonium states are known very well in some cases while very little is known about others. In general, the S-wave ($L = 0$) vector ($S = 1$) $J^{PC} = 1^{--}$ states, such as the J/ψ and Υ, are very well studied since they can be produced directly in e^+e^- annihilation and can thus decay to the experimentally clean e^+e^- and $\mu^+\mu^-$ final states. The P-wave ($L = 1$) spin triplet ($S = 1$) χ states are also reasonably well studied as they are readily produced in the radiative decays of the vector states and can decay to lower lying vector states with the emission of a photon. However, much less is known about the spin singlet ($S = 0$) S-wave states, η_c and η_b, the latter of which ($\eta_b(1S)$) was only recently discovered in 2008 [5]. The di-lepton decays of these states are heavily suppressed, with decays to light hadrons dominating. These states are typically studied through radiative decays of the type $^3S_1 \rightarrow {}^1S_0\gamma$, although this radiative transition is dominated by a magnetic dipole amplitude and is strongly suppressed relative to the analogous electric dipole transition. Less still is known about the spin singlet P-wave states, h_c and h_b, the decays of which are also dominantly hadronic.

The quarkonium spectrum can be understood from a theoretical perspective through two distinct approaches. The first approach is largely phenomenological and involves the use of potential models to describe the bound state, in analogy with the quantum mechanical description of the energy levels of an atom. The potential model approach is attractive because of its simplicity, but becomes steadily more complicated and inaccurate for the heavier quarkonium states (particularly those above the open flavour thresholds). The alternative approach is to perform a direct

calculation using QCD. Such calculations can be performed with lattice QCD but are complex and (very) computationally expensive; few lattice calculations exist relative to the many potential model calculations in the literature. However, lattice calculations that use the effective theory Non-Relativistic QCD (NRQCD) have successfully described much of the charmonium and bottomonium spectrum [7–9].

The main features of the experimentally observed spectrum of quarkonium states can be reproduced with a simple non-relativistic potential model. The use of an interaction potential and "ordinary" non-relativistic quantum mechanics to model the system is well motivated given the large masses of the charm and bottom quarks relative to the QCD scale, Λ_{QCD}. The potential $V(\vec{r})$ can be parameterised as a function of the relative separation, $\vec{r}$, between the quark Q and the anti-quark $\bar{Q}$. The problem is simplified mathematically if one models the system as an anti-quark orbited by a quark with mass μ bound by an attractive relative central potential $V(r)$ (a common technique used in the textbook [10] solution of the Schrödinger equation for the hydrogen atom). The parameter μ is known as the *reduced mass*. As the mass of the heavy quark and anti-quark are equal, the reduced mass is simply $\mu = m_Q/2$, where m_Q is the mass of the heavy quark. If the spin of the quarks is neglected, the binding energy E_{nl} of the bound state can be found by solving the time-independent Schrödinger equation (in natural units with $\hbar = 1$) for the potential,

$$\left[-\frac{\nabla^2}{2\mu} + V(r) \right] \psi_{nlm}(r, \theta, \phi) = E_{nl} \, \psi_{nlm}(r, \theta, \phi) , \qquad (2.1)$$

where θ and ϕ are the polar and azimuthal co-ordinates of the heavy quark [10]. The quantum numbers n, l and m are the principal quantum number, orbital angular momentum quantum number and its projection onto the z-axis respectively. The mass of the quarkonium state is then given by $M_{nl} = E_{nl} + 2m_Q$. The parametrisation of the problem with a spherically symmetric central potential in polar coordinates allows the wavefunction $\psi_{nlm}(r, \theta, \phi)$ to be factorised into a product of three functions, $\psi_{nlm}(r, \theta, \phi) = R_{nl}(r)\Theta_{lm}(\theta)\Phi_m(\phi)$. The product $\Theta_{lm}(\theta)\Phi_m(\phi)$ is described by the spherical harmonic functions $Y_{lm}(\theta, \phi)$ [10]. Thus the total wavefunction is given by $\psi_{nlm}(r, \theta, \phi) = R_{nl}(r)Y_{lm}(\theta, \phi)$. The parametrisation of the solution can be simplified further with the introduction of the *reduced radial wavefunction $u_{nl}(r) = r R_{nl}(r)$*. The Schrödinger equation can then be written as,

$$\frac{d^2 u_{nl}(r)}{dr^2} = \frac{1}{2\mu} \left[E_{nl} - V(r) - \frac{l(l+1)}{2\mu r^2} \right] u_{nl}(r). \qquad (2.2)$$

The boundary conditions $u_{nl}(0) = 0$ and $u'_{nl}(0) = R_{nl}(0)$ must also be imposed to remove unphysical solutions [11]. Finally, the normalisation condition,

$$\int |\psi|^2 r^2 \sin\theta d\theta d\phi dr = \int_0^\infty |u_{nl}(r)|^2 dr = 1 , \qquad (2.3)$$

must also be imposed to preserve unitarity [11].

The form of the potential can be predicted from the qualitative features of QCD. At short distances, less than 1 fm, corresponding to energies greater than the QCD scale, Λ_{QCD}, the potential can be calculated with perturbative QCD. The QCD static potential can be derived from the leading order contribution (single gluon exchange) to the $Q\bar{Q} \rightarrow Q\bar{Q}$ scattering amplitude. This leads to a potential with a form analogous to the Coulomb potential of QED,

$$V(r) = -\mathcal{C}\frac{\alpha_{\text{S}}}{r}, \tag{2.4}$$

where α_{S} is the strong coupling constant and $\mathcal{C}$ is a constant factor related to the colour configuration of the $Q\bar{Q}$ state. For a $Q\bar{Q}$ pair in a colour singlet configuration $\mathcal{C} = 4/3$, while for a colour octet configuration $\mathcal{C} = -1/6$. It is important to note that the overall potential is attractive ($V < 0$) only for the colour singlet configuration, and so $Q\bar{Q}$ pairs in a colour octet configuration can not form bound states, a feature consistent with experimental observations.

At distances beyond around 1 fm, corresponding to energies similar to or less than Λ_{QCD}, the coupling becomes strong, leading to a confinement regime. In this regime, perturbative QCD is no longer valid as α_s is no longer small. Instead, a phenomenologically motivated potential must be used. The most common model is still inspired by the qualitative features of QCD, where a colour field flux tube forms between colour charges separated by large distances, leading to a distance independent confining force [12]. This can be interpreted as a long range linear confining potential,

$$V(r) = Kr, \tag{2.5}$$

where K is a parameter often called the QCD string tension [11]. The parameter K is chosen with input from the experimentally measured spectrum and typically takes values of around 0.18 GeV^2 [12]. This "Coulomb + Linear" potential (alternative parametrisations also exist, such as the Cornell [13] and Richardson [14] potentials) can be used to provide a reasonably good description of the spin-independent features of the experimentally measured charmonium and bottomonium spectra. The QCD static potential can also be calculated to higher perturbative orders to provide a more accurate description which includes an explicit running of the strong coupling. This naturally leads to a confining behaviour at large separations, negating the need for the phenomenologically motivated additional terms [11]. In addition to higher order QCD corrections, corrections to the non-relativistic approximation can also be added to improve the accuracy of the model. Further spin-dependent terms must be included to reproduce the hyperfine splitting between the $^1S_0$ (η_c, η_b) and $^3S_1$ (J/ψ, Υ) states and the fine structure of the P-wave χ states. The addition of terms that model the spin-orbit and hyperfine interactions leads to much more precise predictions that can be directly compared with experimental measurements.

Tables 2.1 and 2.2 show a collection of potential model and lattice QCD predictions for the masses of selected charmonium and bottomonium states. The agreement of modern potential model predictions with the experimental values is very good [15].

Table 2.1 Theoretical predictions for the masses of the charmonium states below the $D\bar{D}$ threshold

Expt. state	$n^{2S+1}L_J$	Expt. mass	Pot. [16]	Pot. [15]	Latt. [7]
$\eta_c(1S)$	1^1S_0	2983.7(7)	2975	2979	3000(2)
J/ψ	1^3S_1	3096.92(1)	3098	3096	Fixed to expt.
h_c	1^1P_1	3525.4(1)	3517	3526	–
χ_{c0}	1^3P_0	3414.8(3)	3445	3424	–
χ_{c1}	1^3P_1	3510.66(7)	3510	3510	–
χ_{c2}	1^3P_2	3556.20(9)	3550	3556	–
$\eta_c(2S)$	2^1S_0	3639.4(1)	3623	3588	3680(6)
$\psi(2S)$	2^3S_1	3686.109(1)	3676	3686	3717(8)

Predictions from potential models (Pot.) [15, 16] and lattice QCD (Latt.) [7] are compared to the world average experimental masses [1]. All masses are quoted in units of MeV

Table 2.2 Theoretical predictions for the masses of the S and P-wave bottomonium states

Expt. state	$n^{2S+1}L_J$	Expt. mass	Pot. [16]	Pot. [15]	Latt. [8]
$\eta_b(1S)$	1^1S_0	9398(3)	9402	9400	9390(9)
$\Upsilon(1S)$	1^3S_1	9460.3(3)	9465	9460	–
$h_b(1P)$	1^1P_1	9899(1)	9882	9901	9905(7)
$\chi_{b0}(1P)$	1^3P_0	9859.4(4)	9847	9865	–
$\chi_{b1}(1P)$	1^3P_1	9892.8(3)	9876	9892	–
$\chi_{b2}(1P)$	1^3P_2	9912.2(3)	9897	9913	–
$\eta_b(2S)$	2^1S_0	9999(4)	9976	9993	9988(3)
$\Upsilon(2S)$	2^3S_1	10023.3(3)	10003	10023	–
$h_b(2P)$	2^1P_1	10259.8(1)	10250	10261	–
$\chi_{b0}(2P)$	2^3P_0	10232.5(5)	10226	10234	–
$\chi_{b1}(2P)$	2^3P_1	10255.5(5)	10246	10255	–
$\chi_{b2}(2P)$	2^3P_2	10268.7(5)	10261	10268	–
$\eta_b(3S)$	3^1S_0	–	10336	10328	–
$\Upsilon(3S)$	3^3S_1	10355.2(5)	10354	10355	10375(22)

Predictions from potential models (Pot.) [15, 16] and lattice QCD (Latt.) [8] are compared to the world average experimental masses [1]. All masses are quoted in units of MeV

Recent lattice QCD results are also in reasonable agreement with data but tend to have larger theoretical uncertainties [7–9].

Within the past ten years, many new states have been observed which decay to quarkonium. These new states, typically denoted by X, Y or Z, have properties that do not obviously fit into the conventional quarkonium model. These states have become known as quarkonium-like states and their nature is still far from well understood. The first such state to be discovered was the $X(3872)$, observed by the Belle experiment in $B^\pm$ meson decays to $J/\psi\,\pi^+\pi^- K^\pm$ final states (with $X(3872) \rightarrow J/\psi\,\pi^+\pi^-$) [17]. The discovery was promptly confirmed by CDF [18] and D0 [19] (in $p\bar{p}$ collisions,

through predominantly prompt production) with several other experiments (including the LHC experiments) subsequently confirming the state's existence. The $X(3872)$ is observed to be a narrow state (with an experimental width consistent with detector resolution) but has a mass above the $D\bar{D}$ threshold. The observation of the $X(3872)$ came as a shock since all known charmonium states with masses above the $D\bar{D}$ threshold are broad states that readily decay to open-charm hadrons. Many theoretical interpretations of the $X(3872)$ have been proposed, including hadronic molecules, tetra-quark states and hybrid charmonium, though its nature is still not firmly established [20]. Since the discovery of the $X(3872)$, many other charmonium-like and bottomonium-like states have also been observed (including manifestly exotic charged states), in multiple final states with varying levels of confirmation [1, 20]. These observations have prompted a significant amount of recent theoretical work. However, to date, no single theoretical interpretation can claim to describe the full spectrum of new states adequately, suggesting that multiple mechanisms may be at play. The LHC experiments and B factories are actively studying these states and new measurements of production cross sections and quantum numbers are beginning to shed more light on these mysterious states [21, 22].

2.2 Quarkonium Production

Quarkonium states can be produced in a variety of different interactions at modern experiments. Common initial states include hadron-hadron collisions (typically pp or $p\bar{p}$ at collider experiments), hadron-nucleon (typically p or $\bar{p}$ on a fixed nuclear target), e^+e^- collisions, $\gamma\gamma$ collisions and ep collisions. The following discussion will focus on the production of quarkonium states in hadronic collisions. Various models describing the production of quarkonium in hadronic collisions exist. The following discussion will attempt to summarise the main models with more emphasis given to the more recent and successful ones.

2.2.1 The QCD Factorisation Method

Particle production in hadronic collisions can be described within QCD in terms of the interactions between the constituent quarks and gluons (also known as partons) within the colliding hadrons. The cross section for the process $H_1(P_1) + H_2(P_2) \rightarrow X$, where $H_{1,2}$ are initial state hadrons with four-momentum $P_{1,2}$ and X is an arbitrary system of final state particles, can be described by,

$$\sigma(P_1, P_2) = \sum_{i,j} \int dx_1 dx_2 f_i(x_1, \mu^2) \cdot f_j(x_2, \mu^2) \cdot \hat{\sigma}_{ij}(p_1, p_2, \alpha_S(\mu^2), Q^2/\mu^2),$$

$$(2.6)$$

Fig. 2.3 A diagram of hard parton-parton scattering within a hadron-hadron collision
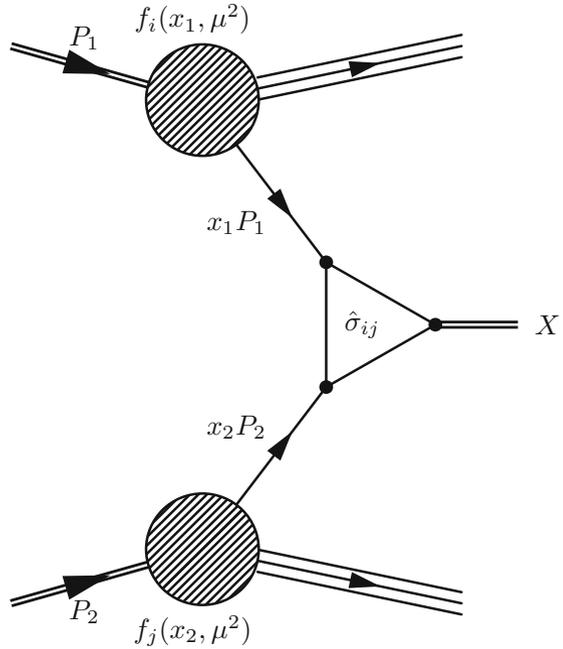
where the indices i, j run over the different parton species within the hadron [23]. This process is shown in diagrammatic form in Fig. 2.3. The quantities $x_{1,2}$ denote the fractions of the initial hadron momenta carried by the partons participating in the hard interaction. Only the longitudinal component of the initial state hadron momentum is considered and the small transverse component is neglected. The momentum of an interacting parton p is then given by $p = xP$. The functions $f_i(x, \mu^2)$ are known as parton distribution functions (PDF) and represent the probability density of finding a parton of species i with momentum fraction x within the parent hadron at a given factorisation scale μ. The partonic cross section $\hat{\sigma}_{ij}$ is the cross section for the scattering of the two partons i and j to produce the system X. The quantity Q is the characteristic scale of the hard scattering, for example the mass of the heavy quark in quarkonium production. The factorisation scale μ is the typical scale below which long distance (low energy) effects dominate and above which short distance (high energy) effects dominate. The factorisation scale is often chosen to be the same as the hard scattering energy scale, $\mu = Q$ [23]. This definition of μ allows the calculation of the total cross section to be factorised into a convolution between PDFs and a partonic cross section $\hat{\sigma}$. Parton behaviour at energy scales below μ, such as the emission of soft gluons, is absorbed into the description of the PDF, negating the need for it to be considered in $\hat{\sigma}$. Through this approach, $\hat{\sigma}$ needs only to describe hard scattering processes for a reliable calculation of inelastic cross sections to be made. The partonic cross section describing the hard parton scattering can be reliably calculated perturbatively, since the strong coupling at the hard scattering

energy scale Q is weak due to asymptotic freedom. It should be noted that the majority of the total inelastic cross section for hadron-hadron interactions represents only soft parton interactions leading to low energy final states. These events must be described in an alternative manner. However, the production of a heavy quark pair (leading to quarkonium production) is a process that is typically well described by the factorisation model.

Examples of proton PDFs for the various parton species are shown in Fig. 2.4, calculated at two different scales. As expected from the quark model of the proton, much of the momentum of the proton is carried by the u and d *valence* quarks, but this does not account for all of the proton's momentum. Fluctuations in the QCD vacuum can lead to the production of $q\bar{q}$ pairs of any flavour within the proton at sufficiently high Q^2. These *sea* quarks do not carry much of the proton momentum but populate a significant fraction of the low x phase space as Q^2 increases. The remaining significant fraction of the proton's momentum is carried by low x gluons. In fact, gluons constitute the dominant contribution in the lowest x region. This is an important feature of the PDF for quarkonium production at a hadron collider. Quarkonium production at central rapidity is typically a low x and low Q^2 process. The momentum transfers $x_{1,2}$ required for a system of mass M at a given centre-of-mass (CM) energy $\sqrt{s}$ are given by $M = \sqrt{x_1 x_2 s}$. For example, at the LHC at $\sqrt{s} = 7$ TeV, the production of a J/ψ with a mass around 3.1 GeV imposes the constraint $x_1 x_2 \approx 2 \times 10^{-7}$. As a consequence of this, gluon initiated quarkonium production forms the dominant contribution to the total production cross section at high energy hadron colliders.
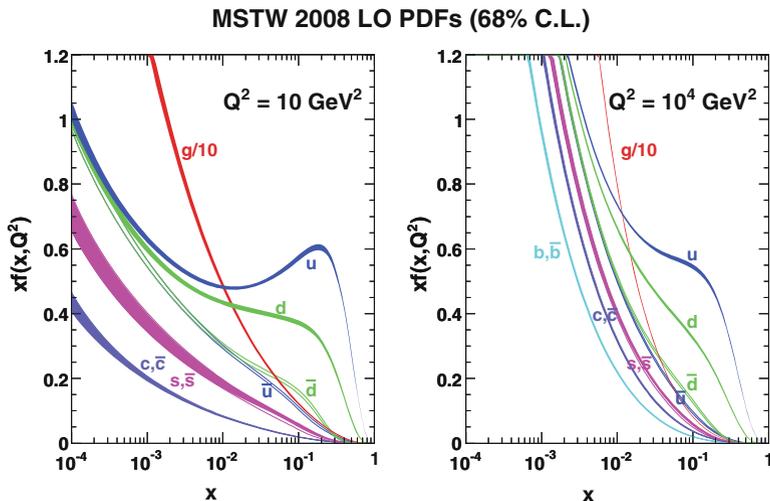
Fig. 2.4 Proton parton distribution functions (PDF), calculated at leading order (LO) in perturbative QCD, for the various parton species calculated by the MSTW group [27]. The PDFs are evaluated at the scales of $Q^2 = 10$ GeV^2 and $Q^2 = 10^4$ GeV^2. The gluon PDF has been scaled down by a factor of 10. Figure from [28]

PDFs are fitted using experimental data. Data collected in a particular process (e.g. jet production at the HERA ep collider) will probe only a particular region of the Q^2 versus x phase space. PDFs can only be useful tools to calculate cross sections if they are known over a wide range of the Q^2 versus x phase space, not necessarily the regions where they are measured experimentally. However, the evolution of the PDFs in Q^2 is known from the Dokshitzer-Gribov-Lipatov-Altarelli-Parisi (DGLAP) equations [24–26]. Thus, a PDF measured as a function of x at a particular value of Q^2 can be evolved to an arbitrary Q^2 (within the perturbative regime and at the expense of some theoretical uncertainty) with the DGLAP equations, allowing cross section predictions to be made in regions of phase space that have not yet been studied experimentally.

Several different approaches have been developed to calculate the partonic cross section, $\hat{\sigma}(ij \rightarrow \mathcal{Q} + X)$, which describes the formation of a quarkonium state $\mathcal{Q}$ through the interaction of the partons i and j. The most phenomenologically successful models will be described in Sects. 2.2.2–2.2.5.

2.2.2 Colour Evaporation Model

The Colour Evaporation Model (CEM) is an early model of quarkonium production (proposed only a few years after the discovery of the J/ψ) but has proved to be rather successful in describing the main features of quarkonium production in hadronic collisions [29–31]. The main ansatz of the CEM is that any $Q\bar{Q}$ pair produced in an hadronic collision will evolve into a quarkonium state if the $Q\bar{Q}$ invariant mass is below the relevant open-flavour threshold ($D\bar{D}$ for charmonium and $B\bar{B}$ for bottomonium). Further to this, it is assumed that the $Q\bar{Q}$ will evolve into a quarkonium state regardless of its spin and colour configuration. Soft gluon interactions (inconsequential to the bulk kinematics of the $Q\bar{Q}$ pair) are assumed to provide the mechanism by which a $Q\bar{Q}$ pair in an arbitrary spin and colour configuration can become arranged into a state with the same quantum numbers as a quarkonium state. For $Q\bar{Q}$ pairs with an invariant mass below the open-flavour threshold, the subsequent probability of the pair to evolve into a particular quarkonium state $\mathcal{Q}$ is given by the fraction $F_\mathcal{Q}$ [12], which is a phenomenologically determined constant, with no dependence on kinematic variables, the quantum numbers of the $Q\bar{Q}$ pair or indeed the $Q\bar{Q}$ production mechanism. While the fractions $F_\mathcal{Q}$ must be extracted from experimental data, they are assumed to be universal (i.e. process independent). Table 2.3 shows the experimentally determined $F_\mathcal{Q}$ parameters for various charmonium and bottomonium states. The resulting model contains no free parameters and is thus very predictive. The leading order cross section for the inclusive production of a quarkonium state $\mathcal{Q}$ in a pp collision is given by,

$$\sigma_{\text{CEM}}(pp \rightarrow \mathcal{Q} + X) = F_\mathcal{Q} \sum_{i,j} \int_{4m_Q^2}^{4M_Q^2} d\hat{s} \int dx_1 dx_2 f_i(x_1, \mu) f_j(x_2, \mu) \hat{\sigma}_{ij}^{Q\bar{Q}}(\hat{s}) \delta(\hat{s} - x_1 x_2 s),$$

$$(2.7)$$

Table 2.3 The CEM parameters $F_{\mathcal{Q}}^{\text{dir.}}$ for the direct production of several charmonium and bottomonium states relative to the inclusive parameters $F_{J/\psi}^{\text{inc.}}$ and $F_{\Upsilon(1S)}^{\text{inc.}}$ respectively

Charmonium State $\mathcal{Q}$	$F_{\mathcal{Q}}^{\text{dir.}}/F_{J/\psi}^{\text{inc.}}$	Bottomonium State $\mathcal{Q}$	$F_{\mathcal{Q}}^{\text{dir.}}/F_{\Upsilon(1S)}^{\text{inc.}}$
J/ψ	0.62	$\Upsilon(1S)$	0.52
$\psi(2S)$	0.14	$\Upsilon(2S)$	0.33
χ_{c1}	0.60	$\Upsilon(3S)$	0.20
χ_{c2}	0.99	$\chi_b(1P)$	1.08
–	–	$\chi_b(2P)$	0.84

The inclusive parameters take values of $F_{J/\psi}^{\text{inc.}} = 0.0144 - 0.0248$ and $F_{\Upsilon(1S)}^{\text{inc.}} = 0.0201 - 0.0508$ where uncertainties in quark masses and PDFs are responsible for the ranges [12]. Parameter values are taken from Refs. [12, 32]

where m_Q is the mass of the heavy quark Q, M_Q is the mass of the lightest meson containing the heavy quark Q [12], $\hat{\sigma}_{ij}^{Q\bar{Q}}$ is the partonic cross section for $ij \rightarrow Q\bar{Q}$ production (where the indices i, j run over the parton species) and $\sqrt{\hat{s}}$ is the partonic centre-of-mass energy. The partonic cross section for $ij \rightarrow Q\bar{Q}$ production is typically calculated in perturbative QCD.

More recent implementations of the CEM have been successful in describing the general features of charmonium production at the Tevatron [33]. However, in other respects the CEM stands in stark contrast with experimental observations. For example, the cross section for χ_c production relative to J/ψ production is considered to be a universal constant, irrespective of the $Q\bar{Q}$ production mechanism. Contrary to this expectation, the available hadroproduction and photoproduction data on this ratio are not in good agreement [12]. The soft interactions that modify the quantum numbers of the initial $Q\bar{Q}$ system are assumed to lead to a uniform distribution of quarkonium spin states, with no particular configuration being preferred. This in turn predicts that the relative direct production rates for quarkonium states with the same orbital angular momentum quantum number, L, are determined by a simple counting of the allowed spin states [12]. For example, this suggests that the direct production rates of the χ_{cJ} states should satisfy the ratios $1 : 3 : 5$ for the $J = 0, 1, 2$ states, respectively. This feature is not observed experimentally; in fact more χ_{c1} is observed to be produced relative to χ_{c2} in hadronic collisions, even after feed-down from $\psi(2S)$ decays is considered [34–36]. Overall, while the CEM successfully reproduces the general characteristics of quarkonium production in hadronic collisions, it consistently fails to describe the majority of the experimental data adequately on a quantitative level [37].

2.2.3 Colour Singlet Model

The colour-singlet model (CSM) is one of the earliest models of quarkonium production and centres around the idea that a $Q\bar{Q}$ pair is produced with the same quantum

numbers as the quarkonium state into which it subsequently evolves [38–41]. Any physical hadronic state is required to be a colour singlet, and thus in the CSM, the $Q\bar{Q}$ pair must be directly produced in a colour singlet state and possessing the spin and angular momentum quantum numbers of the quarkonium state that it will eventually form. The probability for a $Q\bar{Q}$ pair to evolve into a quarkonium state is determined from the values of the colour singlet $Q\bar{Q}$ wavefunction (and its spatial derivatives) evaluated at the origin. These quantities are determined from potential models of the $Q\bar{Q}$ system and are constrained with experimental data on quarkonium decay widths (also related to the wavefunction at the origin). Other than the input on the $Q\bar{Q}$ wavefunction, the CSM contains no free parameters and is thus very predictive [12]. The partonic cross section for the production of a quarkonium state $\mathcal{Q}$ with quantum numbers $^{2S+1}L_J$ is given in the CSM by

$$\hat{\sigma}_{\text{CSM}}(ij \rightarrow \mathcal{Q}\left[^{2S+1}L_J\right] + X) = \left|\frac{d^L\Psi_{nl}(0)}{dr^L}\right|^2 \tilde{\sigma}_{ij}(ij \rightarrow Q\bar{Q}\left[^{2S+1}L_J\right]), \quad (2.8)$$

where Ψ_{nl} is the $Q\bar{Q}$ wavefunction and $\tilde{\sigma}_{ij}$ is the partonic cross section for the interaction of the partons i and j to produce a colour singlet $Q\bar{Q}$ pair with the quantum numbers $^{2S+1}L_J$ [42].

The CSM enjoyed some success in predicting quarkonium production until experimental data from the Tevatron suggested that the CSM significantly underestimated the prompt charmonium cross section in $p\bar{p}$ collisions at $\sqrt{s} = 1.8$ [43] (see Fig. 2.6). The CSM encounters further difficulties in predicting the production and decay of quarkonium states with non-zero orbital angular momentum, such as the $L = 1$ χ states. Such calculations lead to infrared divergences that can only be cancelled through the inclusion of colour-octet contributions [12]. However, several modern proponents of the model exist, with recent calculations, including next-to-leading (NLO) and next-to-next-to-leading (NNLO) corrections in α_S, enjoying improved agreement with experimental data [44]. However, the sizes of these higher order corrections are found to be large, leading to concerns that the perturbative series may not be convergent [20]. As a result of these inconsistencies and its lack of experimental support, many consider the CSM no longer to be a theoretically robust model of quarkonium production.

2.2.4 k_T *Factorisation*

The k_T factorisation method is based upon an alternative procedure used to calculate the inclusive hadron-hadron scattering cross sections, distinct from that discussed in Sect. 2.2.1. The usual approach considers only the longitudinal momentum of the initial state partons and assumes that they possess zero initial transverse momentum; this is known as the collinear factorisation approach. The k_T factorisation approach uses alternative PDFs that include an explicit transverse momentum dependence,

known as unintegrated parton distribution functions (uPDF). These k_T dependent uPDFs are often coupled with a partonic cross section calculated with the CSM. The proponents of this method argue that some of the shortcomings of the CSM are related to the approximations of collinear factorisation and that the use of k_T dependent uPDFs can remedy this [45]. Several predictions exist that significantly improve the agreement of the leading order (LO) CSM with experimental data [46, 47]. However, k_T dependent uPDFs (particularly the gluon distributions) suffer from much larger uncertainties than conventional PDFs and are not well constrained by experimental data.

2.2.5 NRQCD Factorisation

NRQCD factorisation represents the most successful approach to predicting quarkonium production, both in terms of its ability to describe many key experimental results and its theoretical completeness in comparison to earlier approaches [48].

One of the theoretical challenges associated with describing quarkonium production within QCD is the presence of multiple important energy-momentum scales. The heavy quark mass and parton hard-scattering momentum scales are generally significantly larger than Λ_{QCD}. At these scales α_S is generally small enough that perturbative methods can be used. However, other important effects involve inherently low energy processes (such as the evolution of a $Q\bar{Q}$ pair into a physical quarkonium state), which cannot be calculated perturbatively.

The energy-momentum scales relevant to quarkonium production include: the mass of the heavy quark, m_Q; the typical momentum of the heavy quark in the CM frame of a $Q\bar{Q}$ bound state, $m_Q v$ (where v is the velocity of a heavy quark in the CM frame); and the typical binding energy of the $Q\bar{Q}$ pair, approximately $m_Q v^2$ [20]. For charmonium and bottomonium, the heavy quark CM velocity is sufficiently low ($v^2 \approx 0.3$ and $v^2 \approx 0.1$, respectively) that non-relativistic approximations are valid. The final relevant momentum scale is the hard scattering scale, Q^2, which is typically given by the transverse momentum of the produced quarkonium state in hadronic collisions. The momentum scales m_Q and Q^2 are related to short distance effects such as the formation of a $Q\bar{Q}$ pair while the scales $m_Q v$ and $m_Q v^2$ are associated with long distance effects such as hadron formation.

In order to make use of well-founded perturbative calculational techniques, the high momentum (short distance) effects that can be calculated within perturbation theory must be separated from the low momentum effects (long distance) which cannot. This is known as the "factorisation" of effects based on their momentum scale [12]. This factorisation can be achieved through the use of the effective field theory of non-relativistic QCD (NRQCD) [49]. An effective field theory can be considered as an approximate theory which contains only the degrees of freedom necessary to describe phenomena up to a particular scale. The effective theory of NRQCD can be shown to reproduce the results of QCD at momentum scales of $m_Q v$ and below [12].

The inclusive cross section for the direct production of a quarkonium state $\mathcal{Q}$ in proton proton collisions takes the form of a sum over products of short distance coefficients $\tilde{\sigma}_n \left[pp \to Q\bar{Q}^{[n]} \right]$ and long distance matrix elements (LDMEs) $\langle \mathcal{Q} | \mathcal{O}_n | \mathcal{Q} \rangle = \left\langle \mathcal{O}_n^{\mathcal{Q}} (\Lambda) \right\rangle$,

$$\sigma \left(pp \to \mathcal{Q} + X' \right) = \sum_n \tilde{\sigma}_n \left[pp \to Q\bar{Q}^{[n]} + X \right] (\Lambda) \cdot \left\langle \mathcal{O}_n^{\mathcal{Q}} (\Lambda) \right\rangle, \qquad (2.9)$$

where the parameter Λ represents the high energy cut-off scale of the effective theory. The $\tilde{\sigma}_n \left[pp \to Q\bar{Q}^{[n]} \right]$ represent the short distance production cross sections for a $Q\bar{Q}$ pair with colour, spin and angular momentum quantum numbers, n, and can generally be calculated with perturbative QCD. One important feature of this approach is that the $Q\bar{Q}$ pair need not be produced with the same quantum numbers (colour, spin and angular momentum) as the quarkonium state into which it will evolve. Crucially, this allows the $Q\bar{Q}$ pair to be produced in either a colour singlet or a colour octet configuration.

The LDMEs are vacuum expectation values of the four-fermion NRQCD operators, $\mathcal{O}_n$, which represent the probabilities for a $Q\bar{Q}$ pair with a given set of colour, spin and angular momentum quantum numbers, n, to evolve into the quarkonium state $\mathcal{Q}$ plus anything (the quantum numbers of $\mathcal{Q}$ need not be identical to that of the $Q\bar{Q}$ pair). These matrix elements encode all of the non-perturbative physics associated with the evolution of a $Q\bar{Q}$ pair into a quarkonium state [20]. One useful property of the long-distance matrix elements is that they are process independent [12]. While this property has not been proven unambiguously, it is phenomenologically very useful and adds to the predictive power of the NRQCD factorisation approach. However, it is not yet known whether the LDMEs needed for the calculation of quarkonium production can be directly calculated from theory (i.e. with lattice QCD simulations). All present calculations in NRQCD use LDMEs extracted phenomenologically, by fitting experimental data.

The sum in the factorisation formula shown in Eq. 2.9 can be parametrised as an expansion in powers of α_S and v. Calculations in the NRQCD factorisation approach are performed by truncating this expansion at a fixed order in v. After truncation, only a finite number (of the infinite number in Eq. 2.9) of unknown LDMEs contribute, making phenomenological predictions possible [20]. The CSM discussed in Sect. 2.2.3 can be derived from NRQCD factorisation by considering only the colour singlet term from Eq. 2.9, at leading order in v, in which the quantum numbers of the $Q\bar{Q}$ pair are the same as the quarkonium state $\mathcal{Q}$ [20].

The predictive power of the NRQCD factorisation approach relies upon the availability of a set of LDMEs that are complete at a given power in v which also provide useful predictions (i.e. beyond trivial case of the CSM). The symmetries of NRQCD predict several approximate relationships between different LDMEs, which reduces the total number of independent free parameters needed at a given order in v [12, 48].

In the case of operators that have the same $Q\bar{Q}$ angular momentum and colour quantum numbers as the dominant Fock state (eigenstates of the particle number operator) of the corresponding quarkonium state, an approximate relationship exists (up to corrections in v) between some LDMEs and the $Q\bar{Q}$ wavefunctions (and their derivatives) evaluated at the origin (as used in the CSM and in potential models of the quarkonium spectrum) [12]. Two examples of this relationship are shown in Eqs. 2.10 and 2.11, which relate the colour singlet matrix elements for the dominant Fock state for the J/ψ and χ_{cJ} to their wavefunctions Ψ_Q (and derivatives) and a colour factor. These relationships allow the direct extraction of the CSM, formulated in terms of the $Q\bar{Q}$ wavefunctions, from NRQCD.

$$\left\langle \mathcal{O}_1^{J/\psi}\left(^3S_1\right)\right\rangle = \frac{3N_c}{2\pi}\left|\Psi_{J/\psi}(0)\right|^2\left(1+\mathcal{O}(v^4)\right) \tag{2.10}$$

$$\left\langle \mathcal{O}_1^{\chi_{cJ}}\left(^3P_J\right)\right\rangle = (2J+1)\frac{3N_c}{2\pi}\left|\Psi'_{\chi_{cJ}}(0)\right|^2\left(1+\mathcal{O}(v^2)\right) \tag{2.11}$$

The simplest yet non-trivial truncation in v yields four independent matrix elements for an S-wave multiplet (J/ψ and η_c) and two independent matrix elements for a P-wave multiplet (χ_{cJ} and h_c) [12]. The typical choice of S-wave matrix elements is $\left\langle \mathcal{O}_1^{J/\psi}\left(^3S_1\right)\right\rangle, \left\langle \mathcal{O}_8^{J/\psi}\left(^1S_0\right)\right\rangle, \left\langle \mathcal{O}_8^{J/\psi}\left(^3S_1\right)\right\rangle$ and $\left\langle \mathcal{O}_8^{J/\psi}\left(^3P_0\right)\right\rangle$, which enter the expansion in v at orders $1, v^3, v^4$ and v^4 respectively [12]. The P-wave matrix elements are typically chosen to be $\left\langle \mathcal{O}_1^{\chi_{c0}}\left(^3P_0\right)\right\rangle$ and $\left\langle \mathcal{O}_8^{\chi_{c0}}\left(^3S_1\right)\right\rangle$, which both contribute at order v^2 [12]. Together, these matrix elements can be used to calculate the production cross sections for all of the spin states in the S-wave and P-wave multiplets and can thus provide specific predictions for the polarisation of the quarkonium states. It should be noted that separate matrix elements exist for each set of radial excitations, n. For example, the matrix elements for $\psi(2S)$ production differ from the equivalent matrix elements for J/ψ production and must be obtained separately. Many physical observables that can be extracted from experimental data are only sensitive to a linear combination of colour octet matrix elements. The linear combination,

$$M_k^Q = \left\langle \mathcal{O}_8^Q\left(^1S_0\right)\right\rangle + \frac{k}{m_Q}\left\langle \mathcal{O}_8^Q\left(^3P_0\right)\right\rangle \tag{2.12}$$

is often defined to facilitate the extraction of these matrix elements from data (an appropriate value of k is chosen depending on the experimental observable). The matrix elements for charmonium are reasonably well known. Table 2.4 shows a set of NRQCD matrix elements extracted from charmonium production cross sections (differential in transverse momentum) measured by CDF [43, 50], taken from Ref. [51]. The situation for bottomonium production is less clear due to the comparative lack of data and the large and complex feed-down contributions to the $\Upsilon(nS)$ cross sections.

Table 2.4 NRQCD matrix elements for charmonium production extracted from CDF data [43, 50], taken from Ref. [51]

J/ψ	$\left\langle \mathcal{O}_1^{J/\psi}\left(^3S_1\right)\right\rangle$	$\left\langle \mathcal{O}_8^{J/\psi}\left(^3S_1\right)\right\rangle$	$M_{3.5}^{J/\psi}$
	$1.16\ \mathrm{GeV}^3$	$(1.19\pm0.14)\times10^{-2}\ \mathrm{GeV}^3$	$(4.54\pm1.11)\times10^{-2}\ \mathrm{GeV}^3$
$\psi(2S)$	$\left\langle \mathcal{O}_1^{\psi(2S)}\left(^3S_1\right)\right\rangle$	$\left\langle \mathcal{O}_8^{\psi(2S)}\left(^3S_1\right)\right\rangle$	$M_{3.5}^{\psi(2S)}$
	$0.76\ \mathrm{GeV}^3$	$(0.50\pm0.06)\times10^{-2}\ \mathrm{GeV}^3$	$(1.89\pm0.46)\times10^{-2}\ \mathrm{GeV}^3$
χ_{c0}	$\left\langle \mathcal{O}_1^{\chi_{c0}}\left(^3P_0\right)\right\rangle$	$\left\langle \mathcal{O}_8^{\chi_{c0}}\left(^3S_1\right)\right\rangle$	–
	$0.11\ \mathrm{GeV}^3$	$(0.31\pm0.04)\times10^{-2}\ \mathrm{GeV}^3$	–

2.2.6 Charmonium Production in b-hadron Decay

The decays of hadrons containing b quarks represent a significant contribution to charmonium production in hadronic collisions. No analogous process contributes to bottomonium production due to the absence of hadrons containing top quarks. Bottom quarks, and thus b-hadrons, are copiously produced at high energy hadron colliders and the typical inclusive branching fractions for the decays of b-hadrons (H_b) to final states including charmonium states $\mathcal{C}$, $\mathcal{B}(H_b \to \mathcal{C} + X)$ are of order 10^{-3}. The fragmentation of b quarks tends to produce a mixture of ground state and excited b-hadrons (such as the $B^{*(*)}$ mesons). The excited states quickly decay to the ground state mesons, $B^\pm$, B^0, B_s^0, and the weakly decaying b-baryons (e.g. Λ_b), all of which can subsequently decay to final states involving a charmonium state. The fraction of b quarks that fragment into B_c mesons is expected to be very small ($\sim$0.2 % from Tevatron measurements) [1].

Charmonium production from b-hadron decays produced in hadron collisions is typically described with a phenomenological model consisting of a b quark production cross section calculated in perturbative QCD, coupled with a phenomenological or data-driven description of the b quark fragmentation process and b-hadron decay [52]. Thus, the total cross section for the production of the charmonium state $\mathcal{C}$ from b-hadron decay in pp collisions can be given by,

$$\sum_i \left[\tilde{\sigma}(pp \to b + X') \otimes f(b \to H_b^i) \otimes D(H_b^i \to \mathcal{C} + X)\right] \cdot \mathcal{B}(H_b^i \to \mathcal{C} + X),$$

$$(2.13)$$

where the index i runs over the relevant weakly decaying b-hadrons and the $\otimes$ symbol represents a convolution in momentum [52]. The cross section $\tilde{\sigma}$ describes the inclusive production of b quarks in pp collisions and is typically calculated with perturbative QCD. The fragmentation functions $f(b \to H_b)$ give the probability for a b quark to produce a b-hadron H_b with a fraction z of the initial b quark momentum. These functions typically contain a single free parameter which is determined by

Table 2.5 The mixture of b-hadrons measured in $Z \rightarrow b\bar{b}$ decays at LEP and $p\bar{p} \rightarrow b\bar{b} + X$ production at the Tevatron [1]

b-hadron	Fraction (%)		
	LEP $Z \rightarrow b\bar{b}$	Tevatron $p\bar{p} \rightarrow b\bar{b} + X$	Combination
$B^{\pm}$, B^0	40.3 ± 0.9	33.9 ± 3.9	40.1 ± 0.8
B_s^0	10.3 ± 0.9	11.1 ± 1.4	10.5 ± 0.6
b-baryons	9.0 ± 1.5	21.2 ± 6.9	9.3 ± 1.6

The fractions for $B^{\pm}$ and B^0 are considered to be equal (i.e. a factor of 2 is understood in this case such that all of the fractions to sum to unity)

fitting experimental data. Typical analytical forms include the Kartvelishvili function shown in Eq. 2.14 and the Peterson function shown in Eq. 2.15 [53, 54].

$$f(z) = z^{\alpha}(1 - z) \tag{2.14}$$

$$f(z) = \frac{1}{z}\left(1 - \frac{1}{z} - \frac{\epsilon_P}{1 - z}\right)^{-2} \tag{2.15}$$

The b quark fragmentation functions have been precisely measured by the LEP experiments in $Z \rightarrow b\bar{b}$ decays. Typical fitted values for the Peterson and Kartvelishvili parameters are $\epsilon_P = 41.2 \times 10^{-4}$ and $\alpha = 11.9$ [55]. The fragmentation functions are generally only measured for the inclusive mixture of b-hadrons produced in $Z \rightarrow b\bar{b}$ decays and not separately for each individual b-hadron species. The measured b-hadron mixtures produced in $Z \rightarrow b\bar{b}$ decays at LEP and in $p\bar{p} \rightarrow b\bar{b} + X$ production at the Tevatron are shown in Table 2.5. There is a difference between the LEP and Tevatron results, suggesting that the fractions may have some dependence on the average b-quark momentum (around $p \sim m_Z/2$ at LEP, but typically lower at the Tevatron).

The functions $D(H_b \rightarrow C + X)$ are analogous to the b quark fragmentation functions and describe the fraction of the b-hadron momentum carried by the charmonium state C in the decay $H_b \rightarrow C + X$ and are often parametrised in terms of the momentum of the charmonium state in the rest frame of the decaying b-hadron, p^*. These distributions have been measured in the decays of the $B^{\pm}/B^0$ meson mixture produced in $\Upsilon(4S)$ decays at the B factories [56], though no data exist for inclusive B_s^0 or b-baryon decays.

The branching fractions for the inclusive production of charmonium states in the decays of the $B^{\pm}/B^0$ meson mixture produced in $\Upsilon(4S)$ decays have been precisely measured by the CLEO, BaBar and Belle experiments [1]. At hadron collider experiments, where the dominant source of b-hadron production is via b quark fragmentation, the b-hadron mixture, and the corresponding inclusive charmonium branching fractions, are less well known. Several measurements of the branching fractions for the inclusive decays $\mathcal{B}(b \rightarrow J/\psi + X)$ and $\mathcal{B}(b \rightarrow \psi(2S) + X)$ have been made for the b-hadron mixtures produced at LEP, the Tevatron and LHC, though little data

Table 2.6 Branching fractions for the inclusive decays of b-hadron mixtures to final states including charmonium

State	Inclusive branching fraction	
	$B^{\pm/0}$ ($\Upsilon(4S)$ Decays)	$B^{\pm/0}$, B_s^0, b-baryon (LEP, tevatron and LHC)
J/ψ	$(10.94 \pm 0.32) \times 10^{-3}$	$(11.6 \pm 1.0) \times 10^{-3}$
$\psi(2S)$	$(3.07 \pm 0.21) \times 10^{-3}$	$(2.83 \pm 0.29) \times 10^{-3}$
χ_{c1}	$(3.86 \pm 0.27) \times 10^{-3}$	$(14 \pm 4) \times 10^{-3}$
χ_{c2}	$(1.3 \pm 0.4) \times 10^{-3}$	–

Data taken from Ref. [1]

exist for inclusive decays to the χ_c states (none in fact for χ_{c2}). Table 2.6 summarises the world average measurements on inclusive branching fractions for the decays of b-hadron mixtures to final states including charmonium. While the inclusive branching fractions for decay to J/ψ and $\psi(2S)$ from $B^{\pm}$, B^0 and from $B^{\pm}$, B^0, B_s^0, b-baryon mixtures are compatible, the measurements do not agree for χ_{c1}, where the only $B^{\pm}$, B^0, B_s^0, b-baryon measurements are from LEP. This may suggest that the χ_{c1} inclusive branching fractions are more sensitive to the B_s^0 or b-baryon content of the b-hadron mixtures than are the J/ψ and $\psi(2S)$ inclusive branching fractions.

The limited knowledge of the production fractions, fragmentation functions and inclusive branching fractions for the relevant b-hadron species in hadron collider experiments constrains the accuracy with which charmonium production from b-hadron decays can be predicted. Furthermore, the universality of the b-hadron production fractions and inclusive branching fractions measured at LEP and the hadron colliders has not been proven. Several measurements, particularly the b-hadron production fractions shown in Table 2.5, point towards a potential systematic discrepancy and potentially significant source of uncertainty that is often not considered. Nonetheless, modern predictions for charmonium production from b-hadron decay calculated within this semi-phenomenological framework have experienced much success in describing the data from the Tevatron and LHC experiments [52, 57].

2.2.7 Hadron Collider Quarkonium Production Phenomenology

The inclusive production of quarkonium states in hadronic collisions can be separated into two distinct processes: direct production and feed-down. Direct production denotes the production of a quarkonium state "directly" in a hard scattering process, as described in the preceding discussion in this chapter. Feed-down denotes the production of quarkonium states in the decay of other quarkonium states (or b-hadrons in the case of charmonium). The inclusive production of a given quarkonium state in hadronic collisions is often a complicated mixture of direct production and feed-down, particularly for the ground state quarkonia. The total feed-down contribution often represents many individual contributions from various decay chains (e.g. $\psi(2S) \rightarrow J/\psi \pi^+\pi^-$ and $\chi_{cJ} \rightarrow J/\psi \gamma$) and is typically experimentally

indistinguishable from direct production unless the full feed-down decay chain is reconstructed. However, in the case of charmonium production, one major feed-down contribution can be reliably separated. The contribution from the decays of b-hadrons can often be separated experimentally from the inclusive production cross section through an exploitation of the long lifetime of the weakly decaying b-hadrons with an analysis of a suitable decay time variable. The experimentally separated contribution from the decays of b-hadrons is often called the *non-prompt* contribution, while the remainder is referred to as the *prompt* contribution. The distinction between prompt and non-prompt charmonium production is important as the two processes are described theoretically within distinct calculational frameworks. Meaningful comparisons between experimental data and theoretical models of charmonium production can only be made if the prompt/non-prompt separation has been performed. This complication is absent in bottomonium production (though feed-down between bottomonium states is present). At hadron collider experiments, generally only the spin triplet $S = 1$ quarkonium states are studied as they can decay directly to a di-lepton final state or can readily decay to a vector quarkonium state (i.e. the χ states). This situation occurs because the dominantly hadronic final states of the spin singlet $S = 0$ quarkonia cannot be triggered upon due to the very large combinatorial backgrounds, while the di-lepton signature is very clean experimentally.

   The most common quarkonium production observable is the cross section, measured either as an absolute quantity or differentially in an appropriate kinematic variable (typically the transverse momentum and/or (pseudo-)rapidity of the quarkonium state). Absolute and differential cross sections are often very sensitive to various production processes and are usually the primary means through which the validity of theoretical models is tested. The other important observable for quarkonium states with non-zero total angular momentum J (e.g. the $J = 1$ J/ψ and Υ states) is the *polarisation* of the quarkonium. The polarisation is related to the angular momentum eigenstate, J_z, composition of a quarkonium state with respect to an axis z. In general, a quarkonium state $\mathcal{Q}$ with total angular momentum J can be produced in a linear superposition of the allowed angular momentum eigenstates of J_z given by,

$$|\mathcal{Q}\rangle = \sum_{m=-J}^{J} a_m \, |\mathcal{Q}; J, m\rangle \,, \tag{2.16}$$

such that $\hat{J}_z \, |\mathcal{Q}; J, m\rangle = m \, |\mathcal{Q}; J, m\rangle$ and the coefficients a_m satisfy $\sum_m |a_m|^2 = 1$. Different production mechanisms can lead to a preference for quarkonia to be produced in particular angular momentum eigenstates (measured with respect to an appropriate axis) due to angular momentum, parity and helicity conservation (in strong and EM interactions). This sensitivity to the production mechanism makes the quarkonium polarisation a very important observable that often provides information complementary to that accessed through cross section measurements. One example of this sensitivity is the production of a vector ($J^{PC} = 1^{--}$) quarkonium state V through gluon fragmentation ($g \rightarrow Q\bar{Q} \rightarrow V + X$). In the case of an on shell gluon (which must have helicity ± 1), to conserve angular momentum, the quarkonium

Fig. 2.5 The angles relevant
to the measurement of
quarkonium polarisation in
$V \rightarrow \ell^+ \ell^-$ decays. The
angles θ and ϕ are defined in
the quarkonium rest frame.
The production plane is the
plane which contains the
momentum of the colliding
hadrons. Various conventions
determine the direction of
the polarisation axis z.
Figure from Ref. [59]
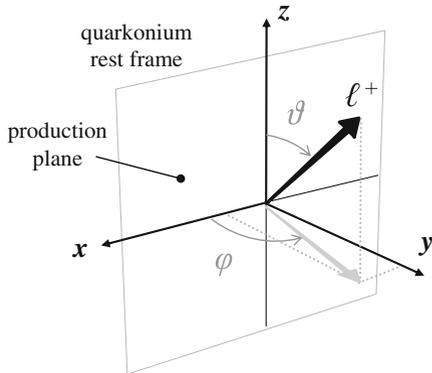
state V must be produced in a state where $J_z = \pm 1$ when measured along the axis
of gluon propagation (approximately the direction of quarkonium propagation, since
X is typically soft).

Quarkonium polarisation is measured experimentally through an analysis of the
angular distributions of the quarkonium decay products. The most common choices
of decay for the measurement of quarkonium polarisation are the di-lepton decays
of the vector quarkonium states $V \rightarrow \ell^+ \ell^-$. The polarisations of the vector states
can also be used to probe the polarisation of the P-wave χ states in the radiative
decays $\chi \rightarrow V \gamma \rightarrow \ell^+ \ell^- \gamma$ [58]. Vector quarkonia are said to have a *transverse*
polarisation if they are in a $J_z = \pm 1$ eigenstate or a *longitudinal* polarisation if in a
$J_z = 0$ eigenstate. Contrary to the nomenclature (adopted in analogy with the photon,
and in reference to the electromagnetic field), the spin vector is aligned along z for
a transverse polarisation and perpendicular to z for a longitudinal polarisation [59].

Figure 2.5 shows the typical system of axes and angles adopted in measurements
of quarkonium polarisation. The polar angle, θ, between the positive lepton and the
polarisation axis, and the azimuthal angle, ϕ, between the positive lepton (in the
V rest frame) and the production plane (also measured in the V rest frame) are
the typical angular observables used in quarkonium polarisation measurements in
$V \rightarrow \ell^+ \ell^-$ decays.

Typical choices of the polarisation axis include the helicity frame (HX), defined
as the quarkonium line of flight in the lab frame, the Collins-Soper frame, defined
as the bisector of the angle between the two hadron momenta in the quarkonium rest
frame, and the Gottfried-Jackson frame, defined as the direction of one of the hadron
momenta in the quarkonium rest frame [59]. In the case of the inclusive production of
V in hadron collisions, the two dimensional angular distribution $W(\theta, \phi)$ is given by

$$W(\theta, \phi) \propto \frac{1}{(3 + \lambda_\theta)} \left[1 + \lambda_\theta \cos^2 \theta + \lambda_\phi \sin^2 \theta \cos 2\phi + \lambda_{\theta\phi} \sin 2\theta \cos \phi \right],$$
(2.17)

where the λ coefficients ($|\lambda| \leq 1$) are related to the angular momentum eigenstate
composition of the produced quarkonia. In the case of pure transverse polarisation

$(J_z = \pm 1)$ $\lambda_\theta = +1$ and $\lambda_\phi = \lambda_{\theta\phi} = 0$, while for longitudinal polarisation $\lambda_\theta = -1$ and $\lambda_\phi = \lambda_{\theta\phi} = 0$.

2.2.7.1 Charmonium Production Phenomenology

Charmonium production at hadron colliders is generally studied with the J/ψ, χ_{cJ} and $\psi(2S)$ states. The J/ψ is the most studied state as it is the most accessible from an experimental perspective. The inclusive production of prompt J/ψ (i.e. neglecting the experimentally separable contribution from b-hadron decays) is composed of three major contributions; direct production, feed-down from radiative χ_c decays and feed-down from the decays of the $\psi(2S)$. The direct contribution is dominant and represents around $(64 \pm 6)\%$ of the cross section [50]. The radiative decays of $\chi_{cJ} \rightarrow J/\psi \gamma$ contribute around $(25 \pm 5)\%$ while the hadronic decays $\psi(2S) \rightarrow J/\psi + X$ (the inclusive branching fraction for such decays is $(60.3 \pm 0.7)\%$ [1]) contribute around $(8.1 \pm 0.3)\%$ [60]. The χ_{cJ} states are studied through their decays $\chi_{cJ} \rightarrow J/\psi \gamma$ and the prompt cross section is predominately direct with a small feed-down contribution from $\psi(2S) \rightarrow \chi_{cJ} \gamma$ decays of around 5% of the total rate [34]. Prompt $\psi(2S)$ production is almost entirely direct due to the absence of any higher mass states below the open-charm threshold.

2.2.7.2 Bottomonium Production Phenomenology

Bottomonium production at hadron colliders is studied with the $\Upsilon(nS)$ and $\chi_b(nP)$ states. The $\Upsilon(nS)$ states are the most studied (similar to the J/ψ for charmonium). The feed-down contributions to the $\Upsilon(1S)$ cross section are complicated and include contributions from the radiative decays of all the χ_b states and the hadronic decays of the $\Upsilon(2, 3S)$ states. The fraction of $\Upsilon(1S)$ produced directly (in $p\bar{p}$ collisions at $\sqrt{s} = 1.8$ TeV) has been measured by CDF to be only $51 \pm 16\%$ [61]. The corresponding fraction for the prompt $\Upsilon(2S)$ cross section has not been measured, but is likely to be similar given the large branching fractions for the decays $\chi_{bJ}(2P) \rightarrow \Upsilon(2S)\gamma)$ (for $J = 1, 2$) and $\Upsilon(3S) \rightarrow \Upsilon(2S)X$, all of which are between 10–20 % [1]. The prompt $\Upsilon(3S)$ cross section was once considered to be fully direct, in analogy with the $\psi(2S)$, though the recent discovery of a candidate for the $\chi_b(3P)$ states now suggests that a possibly significant feed-down contribution may exist [62, 63]. The radiative decays $\Upsilon(nS) \rightarrow \chi_b((n-1)P)\gamma$ are the only dominant feed-down contributions to the prompt $\chi_b(nP)$ cross sections. No data exist on the direct fractions of prompt χ_b production. Radiative Υ decays have branching fractions at the level of between 3 and 13 % [1] (a rate similar to $\psi(2S) \rightarrow \chi_{cJ} \gamma$) and are only expected to contribute at a low level, similar to the situation for χ_c in the charmonium sector.

Fig. 2.6 CDF measurements of charmonium production in $p\bar{p}$ collisions at $\sqrt{s} = 1.8$ TeV. The *upper* figure shows the direct J/ψ production cross section, determined by subtracting contributions from χ_c and $\psi(2S)$ feed-down. The *middle* figure shows the prompt $\psi(2S)$ production cross section while the lower figure shows the contribution to the prompt J/ψ production cross section from radiative χ_c decays. The differential cross sections in each figure are compared with the prediction from NRQCD (the sum of all individual curves, denoted total) and the CSM. All figures from Ref. [51]
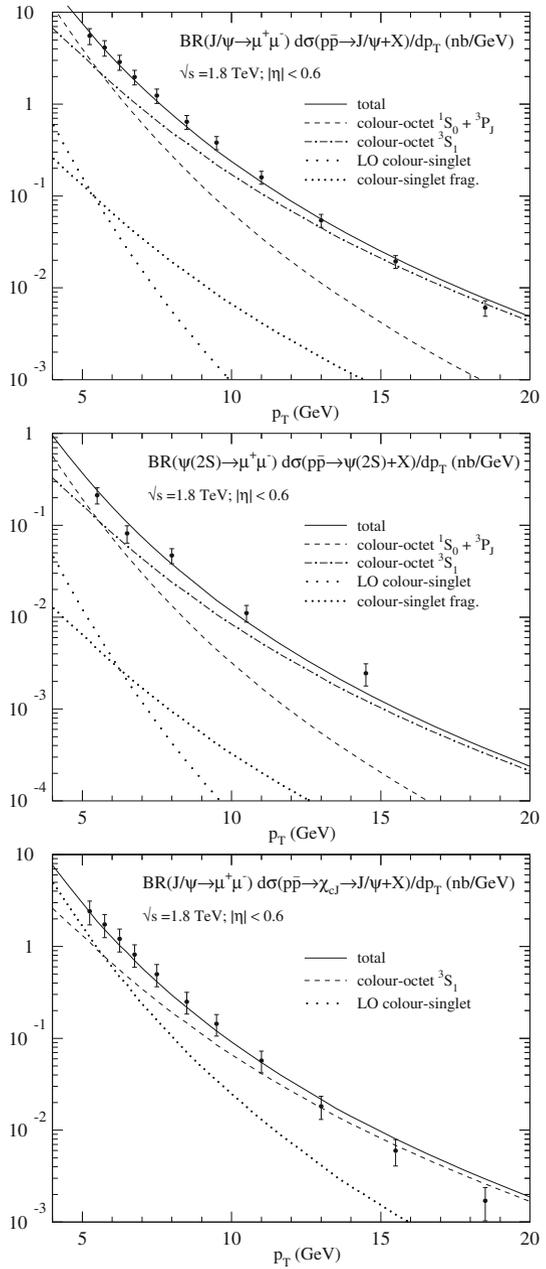
2.2.8 Quarkonium Production Measurements at the Tevatron

The cross sections for the production of prompt J/ψ, $\psi(2S)$ and χ_c were measured by CDF in $p\bar{p}$ collisions at $\sqrt{s} = 1.8$ TeV at the Tevatron in Run I (see Fig. 2.6) [43, 50]. All of the dominant contributions to prompt J/ψ production were determined and an estimate of the direct J/ψ production cross section was made. Production cross section measurements for the J/ψ and $\psi(2S)$ states were also performed with the much larger Tevatron Run II dataset collected at $\sqrt{s} = 1.96$ TeV [64, 65]. The D0 experiment also performed similar measurements with the Tevatron Run I dataset [66]. The measured prompt J/ψ cross sections were found to be over an order of magnitude greater than the expectations of the CSM, prompting a renaissance in theoretical models. NRQCD based predictions were subsequently found to be in much better agreement with the measurements. No measurements of the absolute χ_c production cross sections were performed with the Tevatron Run II dataset ($\sqrt{s} = 1.96$ TeV) though a measurement of the relative prompt production cross section $\sigma(\chi_{c2})/\sigma(\chi_{c1})$ was made [34]. This measurement was the first to contradict strongly the expectations of the CSM and CEM, measuring a χ_{c1} cross section in excess of that of χ_{c2}. The prompt and non-prompt J/ψ and $\psi(2S)$ polarisations were measured with the Tevatron Run II dataset by CDF [67]. CDF measured a small longitudial polarisation for prompt J/ψ production, in disagreement with the NRQCD prediction of a strong transverse polarisation which increases with transverse momentum.

The production cross sections for the $\Upsilon(nS)$ states in $\sqrt{s} = 1.8$ TeV $p\bar{p}$ collisions were measured by both D0 [68] and CDF [69] using the Tevatron Run I dataset. Both measurements are well described by NRQCD based predictions in the high transverse momentum region [51]. The polarisations of the $\Upsilon(nS)$ states were also measured by D0 [70] and CDF [71] with the Tevatron Run II dataset ($\sqrt{s} = 1.96$ TeV). Both experiments observed a longitudinal polarisation. CDF measured only a slight longitudinal polarisation for $\Upsilon(1S)$ production ($-0.23 < \lambda_\theta < 0.01$), though D0 measured a much stronger longitudinal polarisation with a contradictory transverse momentum dependence. The measurement of only the polar angle θ in $\Upsilon \to \mu^+\mu^-$ decays (integrating over the azimuthal angle ϕ) and the use of frame dependent quantities has been suggested as the source of this discrepancy [59]. Neither of the measurements supports the NRQCD prediction of a transverse polarisation.

2.2.9 Quarkonium Production Measurements at the LHC

All of the LHC experiments have now contributed measurements of quarkonium production at a variety of CM energies. The production cross sections for both prompt and non-prompt J/ψ have been measured by all of the LHC experiments in pp collisions at $\sqrt{s} = 7$ TeV [72–75] and at $\sqrt{s} = 8$ TeV [76]. The CMS and LHCb experiments have also measured the prompt and non-prompt $\psi(2S)$ production cross
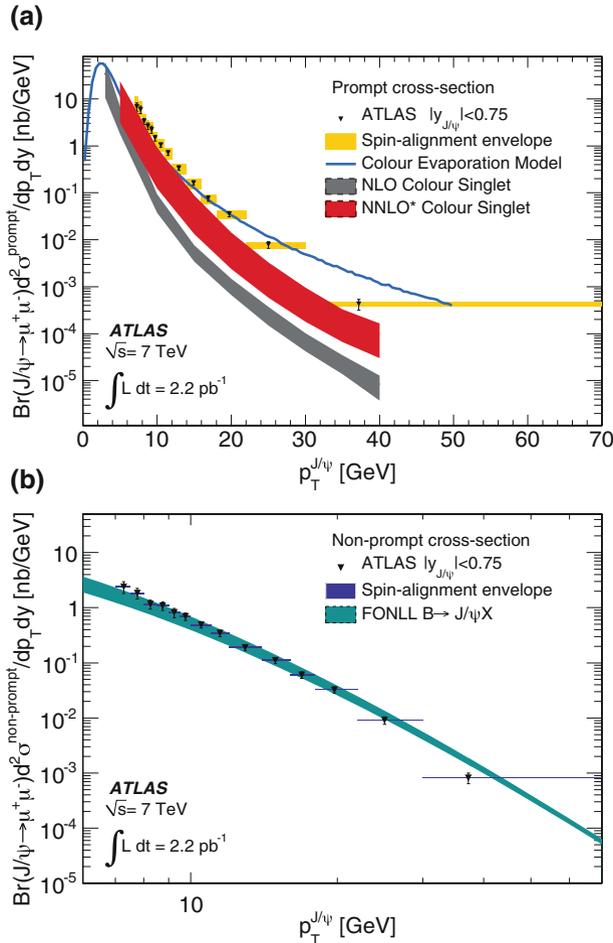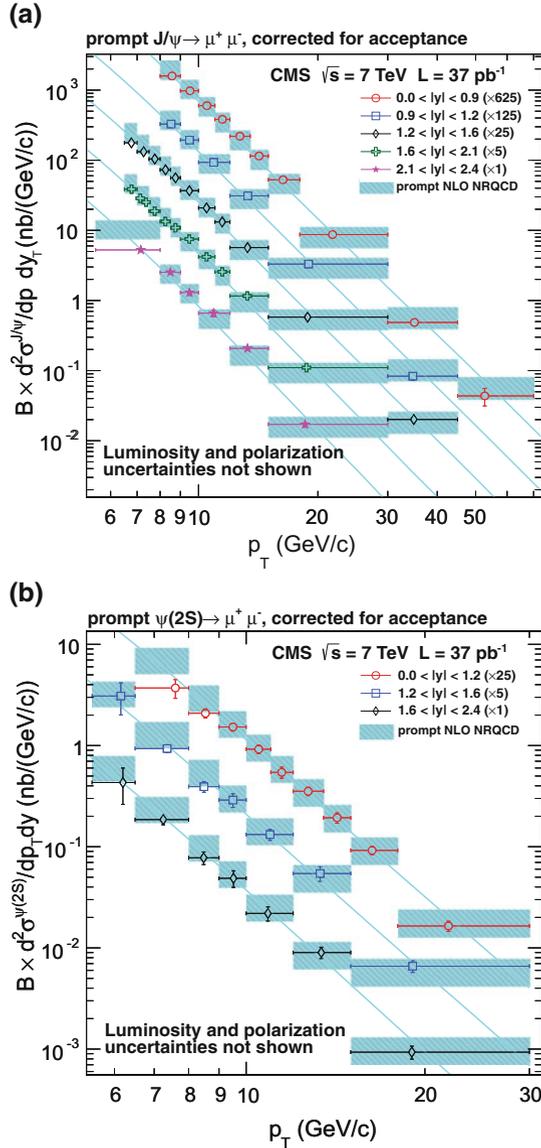
(a)

(b)

Fig. 2.7 The cross sections for prompt **a** and non-prompt **b** J/ψ production in pp collisions at $\sqrt{s} = 7$ TeV measured by ATLAS [73]. The measurements of the prompt cross sections are compared to the predictions of the CEM and the CSM while the non-prompt cross section is compared to the predictions of the FONLL approach [52]

sections at $\sqrt{s} = 7$ TeV [74, 77]. The ATLAS, CMS and LHCb J/ψ and $\psi(2S)$ differential cross section measurements are shown in Figs. 2.7, 2.8 and 2.9 respectively. The fraction of prompt J/ψ produced in the radiative decays $\chi_{cJ} \rightarrow J/\psi \gamma$ was measured at $\sqrt{s} = 7$ TeV to be between 14.0 % at low J/ψ transverse momentum (3 GeV) rising to 26.8 % at higher transverse momentum (14 GeV) [78]. The production cross section of χ_{c2} relative to χ_{c1} has also been measured by CMS [36] and LHCb [35], confirming the CDF observation of $\sigma(\chi_{c1}) > \sigma(\chi_{c2})$. In general, all of the prompt charmonium production cross sections measured at the LHC are well described by NRQCD predictions (with LDMEs extracted from Tevatron data). The

Fig. 2.8 The cross sections for prompt J/ψ **a** and $\psi(2S)$ **b** production in pp collisions at $\sqrt{s} = 7$ TeV measured by CMS [74]. The measurements are compared to the predictions of NLO NRQCD

ALICE, CMS and LHCb experiments have all measured the polarisation of promptly produced J/ψ [79–81]. All of the experiments measure only a weak polarisation, consistent with zero in some regions of phase space. The CMS experiment has also measured the polarisation of promptly produced $\psi(2S)$ to be similarly weak [79]. These observations further increase the disagreement with the NRQCD predictions of a strong transverse polarisation.

(a)

(b)
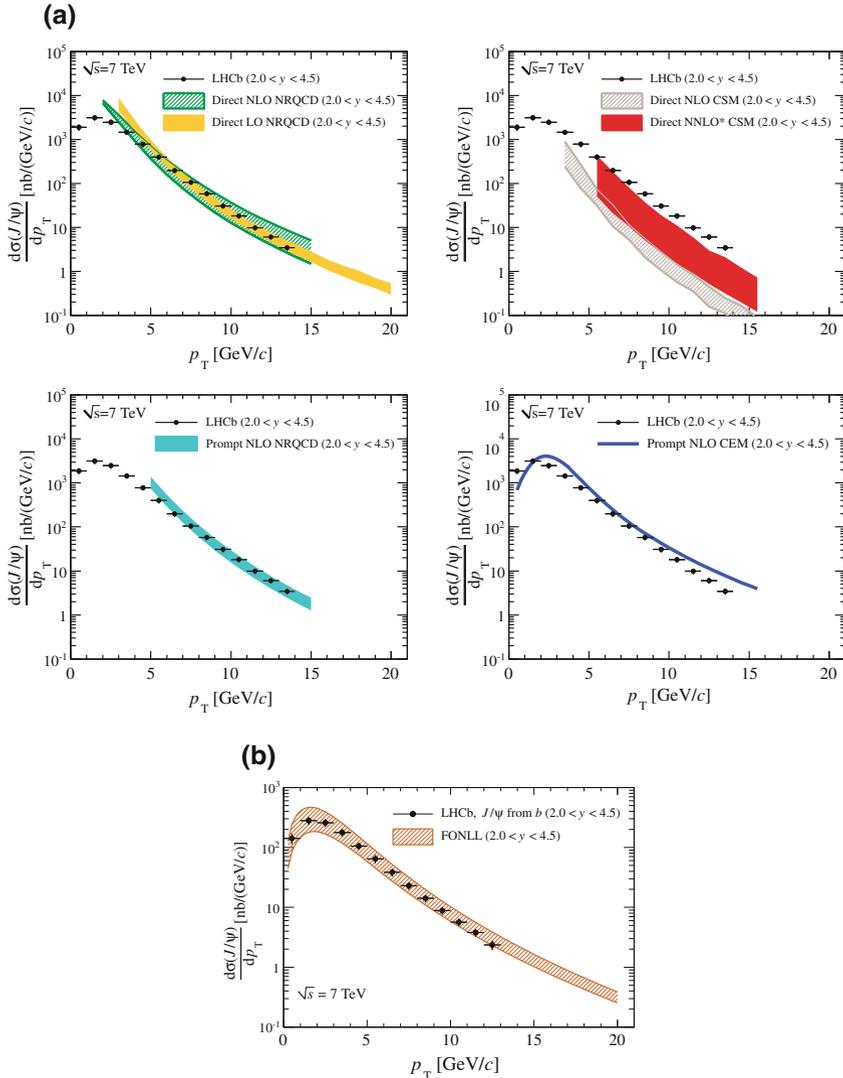
Fig. 2.9 The cross sections for prompt J/ψ production in pp collisions at $\sqrt{s} = 7$ TeV measured by LHCb [75]. The measurements of the prompt cross sections **a** are compared to the predictions of NRQCD and the CSM while the non-prompt cross section **b** is compared to the predictions of the FONLL approach [52]

In addition to measurements of inclusive charmonium production, the LHCb experiment has measured the cross sections for the exclusive production of charmonium states in pp collisions [82]. The exclusive production of charmonium states in pp interactions is a diffractive process that proceeds through photon and colour

singlet (pomeron) exchanges between the intial state protons. Such measurements are useful probes of the very low-x gluon distribution ($x \sim 10^{-6}$) in the proton PDF, a region of phase space difficult to access in inelastic pp interactions.

The ATLAS, CMS and LHCb experiments have measured the cross sections for $\Upsilon(nS)$ production at $\sqrt{s} = 7$ TeV [83–85] and at $\sqrt{s} = 8$ TeV [76]. The LHCb experiment has measured the fraction of $\Upsilon(1S)$ produced in radiative $\chi_b(1P)$ decays to be around 20 % and largely independent of $\Upsilon(1S)$ transverse momentum [86]. The CMS experiment has measured the $\Upsilon(nS)$ polarisation to be slightly transverse, with sequentially stronger transverse polarisation for the $\Upsilon(2S)$ and $\Upsilon(3S)$ states [87].

References

1. J. Beringer et al., Particle Data Group, Review of particle physics (RPP). Phys. Rev. D **86**, 010001 (2012)
2. J.E. Augustin et al., SLAC-SP-017 Collaboration, Discovery of a narrow resonance in e^+e^- annihilation. Phys. Rev. Lett. **33**, 1406–1408 (1974)
3. J.J. Aubert et al., E598 Collaboration, Experimental observation of a heavy particle. J. Phys. Rev. Lett. **33**, 1404–1406 (1974)
4. S.W. Herb et al., Observation of a dimuon resonance at 9.5 GeV in 400 GeV proton—nucleus collisions. Phys. Rev. Lett. **39**, 252–255 (1977)
5. B. Aubert et al., BaBar Collaboration, Observation of the bottomonium ground state in the decay $\Upsilon(3S) \to \gamma\eta_b$. Phys. Rev. Lett. **101**, 071801 (2008). [arXiv:0807.1086]
6. R. Mizuk et al., Evidence for the $\eta_b(2S)$ and observation of $h_b(1P) \to \eta_b(1S)\gamma$ and $h_b(2P) \to \eta_b(1S)\gamma$. Phys. Rev. Lett. **109**, 232002 (2012). [arXiv:1205.6351]
7. C. Davies, K. Hornbostel, G. Lepage, A. Lidsey, J. Shigemitsu et al., Precision charmonium spectroscopy from lattice QCD. Phys. Rev. D **52**, 6519–6529 (1995). [hep-lat/9506026]
8. R. Dowdall et al., HPQCD Collaboration, The Upsilon spectrum and the determination of the lattice spacing from lattice QCD including charm quarks in the sea. Phys. Rev. D **85**, 054509 (2012). [arXiv:1110.6887]
9. J. Daldrop, C. Davies, R. Dowdall, HPQCD Collaboration, Prediction of the bottomonium D-wave spectrum from full lattice QCD. Phys. Rev. Lett. **108**, 102003 (2012). [arXiv:1112.2590]
10. R. Eisberg, R. Resnick, *Quantum Physics*, 2nd edn. (Wiley, 1985)
11. S. Narison, *QCD as a Theory of Hadrons: From Partons to Confinement* (Cambridge University Press, Cambridge, 2002)
12. N. Brambilla et al., Quarkonium Working Group, *Heavy quarkonium physics*. [hep-ph/0412158]
13. E. Eichten, K. Gottfried, T. Kinoshita, K. Lane, T.-M. Yan, Charmonium: the model. Phys. Rev. D **17**, 3090 (1978)
14. J.L. Richardson, The heavy quark potential and the Υ, J/ψ systems. Phys. Lett. B **82**, 272 (1979)
15. D. Ebert, R. Faustov, V. Galkin, Properties of heavy quarkonia and B_c mesons in the relativistic quark model. Phys. Rev. D **67**, 014027 (2003). [hep-ph/0210381]
16. S. Godfrey, N. Isgur, Mesons in a relativized quark model with chromodynamics. Phys. Rev. D **32**, 189–231 (1985)
17. S. Choi et al., Belle Collaboration, Observation of a narrow charmonium-like state in exclusive $B^\pm \to K^\pm \pi^+\pi^- J/\psi$ decays. Phys. Rev. Lett. **91**, 262001 (2003). [hep-ex/0309032]
18. D. Acosta et al., CDF Collaboration, Observation of the narrow state $X(3872) \to J/\psi\pi^+\pi^-$ in $\bar{p}p$ collisions at $\sqrt{s} = 1.96$ TeV. Phys. Rev. Lett. **93**, 072001 (2004). [hep-ex/0312021]

19. V. Abazov et al., D0 Collaboration, Observation and properties of the $X(3872)$ decaying to $J/\psi\pi^+\pi^-$ in $p\bar{p}$ collisions at $\sqrt{s} = 1.96$ TeV. Phys. Rev. Lett. **93**, 162002 (2004). [hep-ex/0405004]
20. N. Brambilla, S. Eidelman, B. Heltsley, R. Vogt, G. Bodwin et al., Heavy quarkonium: progress, puzzles, and opportunities. Eur. Phys. J. C **71**, 1534 (2011). [arXiv:1010.5827]
21. R. Aaij et al., LHCb Collaboration, Determination of the $X(3872)$ meson quantum numbers. Phys. Rev. Lett. **110**, 222001 (2013). [arXiv:1302.6269]
22. S. Chatrchyan et al., CMS Collaboration, Measurement of the $X(3872)$ production cross section via decays to $J/\psi\pi^+\pi^-$ in pp collisions at $\sqrt{s} = 7$ TeV. JHEP **1304**, 154 (2013). [arXiv:1302.3968]
23. R.K. Ellis, W.J. Stirling, B.R. Webber, *QCD and Collider Physics* (Cambridge University Press, Cambridge, 1996)
24. V. Gribov, L. Lipatov, Deep inelastic *ep* scattering in perturbation theory. Sov. J. Nucl. Phys. **15**, 438–450 (1972)
25. G. Altarelli, G. Parisi, Asymptotic freedom in parton language. Nucl. Phys. B **126**, 298 (1977)
26. Y.L. Dokshitzer, Calculation of the structure functions for deep inelastic scattering and e^+e^- Annihilation by perturbation theory in quantum chromodynamics. Sov. Phys. JETP **46**, 641–653 (1977)
27. A. Martin, W. Stirling, R. Thorne, G. Watt, Parton distributions for the LHC. Eur. Phys. J. C **63**, 189–285 (2009). [arXiv:0901.0002]
28. MSTW Parton Distribution Function figures http://mstwpdf.hepforge.org/. Accessed 22 Jan 2014
29. H. Fritzsch, Producing heavy quark flavors in hadronic collisions: a test of quantum chromodynamics. Phys. Lett. B **67**, 217 (1977)
30. F. Halzen, CVC For gluons and hadroproduction of quark flavors. Phys. Lett. B **69**, 105 (1977)
31. M. Gluck, J. Owens, E. Reya, Gluon contribution to hadronic J/ψ production. Phys. Rev. D **17**, 2324 (1978)
32. S. Digal, P. Petreczky, H. Satz, Quarkonium feed down and sequential suppression. Phys. Rev. D **64**, 094015 (2001). [hep-ph/0106017]
33. J. Amundson, O.J. Eboli, E. Gregores, F. Halzen, Quantitative tests of color evaporation: charmonium production. Phys. Lett. B **390**, 323–328 (1997). [hep-ph/9605295]
34. A. Abulencia et al., CDF Collaboration, Measurement of $\sigma_{\chi_{c2}}\mathcal{B}(\chi_{c2} \to J/\psi\gamma)/\sigma_{\chi_{c1}}\mathcal{B}(\chi_{c1} \to J/\psi\gamma)$ in $p\bar{p}$ collisions at $\sqrt{s} = 1.96$ TeV. Phys. Rev. Lett. **98**, 232001 (2007). [hep-ex/0703028]
35. R. Aaij et al., LHCb Collaboration, Measurement of the cross-section ratio $\sigma(\chi_{c2})/\sigma(\chi_{c1})$ for prompt χ_{c1} production at $\sqrt{s} = 7$ TeV. Phys. Lett. B **714**, 215–223 (2012). [arXiv:1202.1080]
36. S. Chatrchyan et al., CMS Collaboration, Measurement of the relative prompt production rate of χ_{c2} and χ_{c1} in pp collisions at $\sqrt{s} = 7$ TeV. Eur. Phys. J. C **72**, 2251 (2012). [arXiv:1210.0875]
37. G.T. Bodwin, E. Braaten, J. Lee, Comparison of the color-evaporation model and the NRQCD factorization approach in charmonium production. Phys. Rev. D **72**, 014004 (2005). [hep-ph/0504014]
38. R. Baier, R. Ruckl, Hadronic production of J/ψ and Υ: transverse momentum distributions. Phys. Lett. B **102**, 364 (1981)
39. R. Baier, R. Ruckl, Hadronic collisions: a quarkonium factory. Z. Phys. C **19**, 251 (1983)
40. E.L. Berger, D.L. Jones, Inelastic photoproduction of J/ψ and Υ by gluons. Phys. Rev. D **23**, 1521–1530 (1981)
41. C.-H. Chang, Hadronic production of J/ψ associated with a gluon. Nucl. Phys. B **172**, 425–434 (1980)
42. G.A. Schuler, Quarkonium production and decays. Phys. Rep. (1994). [hep-ph/9403387]
43. F. Abe et al., CDF Collaboration, J/ψ and $\psi(2S)$ production in $p\bar{p}$ collisions at $\sqrt{s} = 1.8$ TeV. Phys. Rev. Lett. **79**, 572–577 (1997)
44. J. Lansberg, J/ψ production at $\sqrt{s} = 1.96$ and 7 TeV: color-singlet model, NNLO* and polarisation. J. Phys. G **38**, 124110 (2011). [arXiv:1107.0292]

45. P. Hagler, R. Kirschner, A. Schafer, L. Szymanowski, O. Teryaev, Towards a solution of the charmonium production controversy: k^- perpendicular factorization versus color octet mechanism. Phys. Rev. Lett. **86**, 1446–1449 (2001). [hep-ph/0004263]

46. S. Baranov, A. Lipatov, N. Zotov, Prompt J/ψ production at LHC: new evidence for the k_t-factorization. Phys. Rev. D **85**, 014034 (2012). [arXiv:1108.2856]

47. S. Baranov, On the $\sigma(\chi_{c2})/\sigma(\chi_{c1})$ ratio in the k_T-factorization approach. Phys. Rev. D **83**, 034035 (2011)

48. G.T. Bodwin, E. Braaten, G.P. Lepage, Rigorous QCD analysis of inclusive annihilation and production of heavy quarkonium. Phys. Rev. D **51**, 1125–1171 (Feb, 1995)

49. W. Caswell, G. Lepage, Effective lagrangians for bound state problems in QED, QCD, and other field theories. Phys. Lett. B **167**, 437 (1986)

50. F. Abe et al., CDF Collaboration, Production of J/ψ mesons from χ_c meson decays in $p\bar{p}$ collisions at $\sqrt{s} = 1.8$ TeV. Phys. Rev. Lett. **79**, 578–583 (1997)

51. M. Kramer, Quarkonium production at high-energy colliders. Prog. Part. Nucl. Phys. **47**, 141–201 (2001). [hep-ph/0106120]

52. M. Cacciari, S. Frixione, N. Houdeau, M.L. Mangano, P. Nason et al., Theoretical predictions for charm and bottom production at the LHC. JHEP **1210**, 137 (2012). [arXiv:1205.6344]

53. V. Kartvelishvili, A. Likhoded, V. Petrov, On the fragmentation functions of heavy quarks into hadrons. Phys. Lett. B **78**, 615 (1978)

54. C. Peterson, D. Schlatter, I. Schmitt, P.M. Zerwas, Scaling violations in Inclusive e^+e^- annihilation spectra. Phys. Rev. D **27**, 105 (1983)

55. G. Abbiendi et al., OPAL Collaboration, Inclusive analysis of the b decays at LEP. Eur. Phys. J. C **29**, 463–478 (2003). [hep-ex/0210031]

56. BaBar Collaboration, Study of inclusive production of charmonium mesons in b decays. Phys. Rev. D **67**, 032002 (Feb, 2003)

57. B.A. Kniehl, G. Kramer, Inclusive J/ψ and $\psi(2S)$ production from B decay in $p\bar{p}$ collisions. Phys. Rev. D **60**, 014006 (1999). [hep-ph/9901348]

58. P. Faccioli, C. Lourenco, J. Seixas, H.K. Wohri, Determination of χ_c and χ_b polarizations from dilepton angular distributions in radiative decays. Phys. Rev. D **83**, 096001 (2011). [arXiv:1103.4882]

59. P. Faccioli, C. Lourenco, J. Seixas, H.K. Wohri, Towards the experimental clarification of quarkonium polarization. Eur. Phys. J. C **69**, 657–673 (2010). [arXiv:1006.2738]

60. P. Faccioli, C. Lourenco, J. Seixas, H. Woehri, Study of ψ' and χ_c decays as feed-down sources of J/ψ hadro-production. JHEP **0810**, 004 (2008). [arXiv:0809.2153]

61. T. Affolder et al., CDF Collaboration, Production of $\Upsilon(1S)$ mesons from χ_b decays in $p\bar{p}$ collisions at $\sqrt{s} = 1.8$ TeV. Phys. Rev. Lett. **84**, 2094–2099 (2000). [hep-ex/9910025]

62. G. Aad et al., ATLAS Collaboration, Observation of a new χ_b state inradiative transitions to $\Upsilon(1S)$ and $\Upsilon(2S)$ at ATLAS. Phys. Rev. Lett. **108**, 152001 (2012). [arXiv:1112.5154]

63. S. Baranov, Prompt $\Upsilon(nS)$ production at the LHC in view of the k_t-factorization approach. Phys. Rev. D **86**, 054015 (2012)

64. D. Acosta et al., CDF Collaboration, Measurement of the J/ψ meson and b–hadron production cross sections in $p\bar{p}$ collisions at $\sqrt{s} = 1960$ GeV. Phys. Rev. D **71**, 032001 (2005). [hep-ex/0412071]

65. T. Aaltonen et al., CDF Collaboration, Production of $\psi(2S)$ mesons in $p\bar{p}$ collisions at $\sqrt{s} = 1.96$ TeV. Phys. Rev. D **80**, 031103 (2009). [arXiv:0905.1982]

66. S. Abachi et al., D0 Collaboration, J/ψ production in $p\bar{p}$ collisions at $\sqrt{s} = 1.8$ TeV. Phys. Lett. B **370**, 239–248 (1996)

67. A. Abulencia et al., CDF Collaboration, Polarization of J/ψ and $\psi(2S)$ mesons produced in $p\bar{p}$ collisions at $\sqrt{s} = 1.96$ TeV. Phys. Rev. Lett. **99**, 132001 (2007). [arXiv:0704.0638]

68. V. Abazov et al., D0 Collaboration, Measurement of inclusive differential cross sections for $\Upsilon(1S)$ production in $p\bar{p}$ collisions at $\sqrt{s} = 1.96$ TeV. Phys. Rev. Lett. **94**, 232001 (2005). [hep-ex/0502030]

69. D. Acosta et al., CDF Collaboration, Υ production and polarization in $p\bar{p}$ collisions at $\sqrt{s} = 1.8$ TeV. Phys. Rev. Lett. **88**, 161802 (2002)

70. V. Abazov et al., D0 Collaboration, Measurement of the polarization of the $\Upsilon(1S)$ and $\Upsilon(2S)$ states in $p\bar{p}$ collisions at $\sqrt{s} = 1.96$ TeV. Phys. Rev. Lett. **101**, 182004 (2008). [arXiv:0804.2799]
71. T. Aaltonen et al., CDF Collaboration, Measurements of angular distributions of muons from Υ meson decays in $p\bar{p}$ collisions at $\sqrt{s} = 1.96$ TeV. Phys. Rev. Lett. **108**, 151802 (2012). [arXiv:1112.1591]
72. K. Aamodt et al., ALICE Collaboration, Rapidity and transverse momentum dependence of inclusive J/ψ production in pp collisions at $\sqrt{s} = 7$ TeV. Phys. Lett. B **704**, 442–455 (2011). [arXiv:1105.0380]
73. G. Aad et al., ATLAS Collaboration, Measurement of the differential cross-sections of inclusive, prompt and non-prompt J/ψ production in proton-proton collisions at $\sqrt{s} = 7$ TeV. Nucl. Phys. B **850**, 387–444 (2011). [arXiv:1104.3038]
74. S. Chatrchyan et al., CMS Collaboration, J/ψ and $\psi(2S)$ production in pp collisions at $\sqrt{s} = 7$ TeV. JHEP **1202**, 011 (2012). [arXiv:1111.1557]
75. R. Aaij et al., LHCb Collaboration, Measurement of J/ψ production in pp collisions at $\sqrt{s} = 7$ TeV. Eur. Phys. J. C **71**, 1645 (2011). [arXiv:1103.0423]
76. R. Aaij et al., LHCb Collaboration, Production of J/ψ and Υ mesons in pp collisions at $\sqrt{s} = 8$ TeV. JHEP **1306**, 064 (2013). [arXiv:1304.6977]
77. R. Aaij et al., LHCb Collaboration, Measurement of $\psi(2S)$ meson production in pp collisions at $\sqrt{s} = 7$ TeV. Eur. Phys. J. C **72**, 2100 (2012). [arXiv:1204.1258]
78. R. Aaij et al., LHCb Collaboration, Measurement of theratio of prompt χ_c to J/ψ production in pp collisions at $\sqrt{s} = 7$ TeV. Phys. Lett. B **718**, 431–440 (2012). [arXiv:1204.1462]
79. S. Chatrchyan et al., CMS Collaboration, Measurement of the prompt J/ψ and $\psi(2S)$ polarizations in pp collisions at $\sqrt{s} = 7$ TeV. Phys. Lett. B **727**, 381–402 (2013). [arXiv:1307.6070]
80. R. Aaij et al., LHCb Collaboration, Measurement of J/ψ polarization in pp collisions at $\sqrt{s} = 7$ TeV. Eur. Phys. J. C **73**, 2631 (2013). [arXiv:1307.6379]
81. B. Abelev et al., ALICE Collaboration, J/ψ polarization in pp collisions at $\sqrt{s} = 7$ TeV. Phys. Rev. Lett. **108**, 082001 (2012). [arXiv:1111.1630]
82. R. Aaij et al., LHCb collaboration, Updated measurements of exclusive J/ψ and $\psi(2S)$ production cross-sections in pp collisions at $\sqrt{s} = 7$ TeV. [arXiv:1401.3288]
83. G. Aad et al., ATLAS Collaboration, Measurement of Υ production in $\sqrt{s} = 7$ TeV pp collisions at ATLAS. Phys. Rev. D **87**, 5 052004 (2013). [arXiv:1211.7255]
84. S. Chatrchyan et al., CMS Collaboration, Measurement of the $\Upsilon(1S)$, $\Upsilon(2S)$, and $\Upsilon(3S)$ cross sections in pp collisions at $\sqrt{s} = 7$ TeV. Phys. Lett. B **727**, 101–125 (2013). [arXiv:1303.5900]
85. R. Aaij et al., LHCb Collaboration, Measurement of Υ production in pp collisions at $\sqrt{s} = 7$ TeV. Eur. Phys. J. C **72**, 2025 (2012). [arXiv:1202.6579]
86. R. Aaij et al., LHCb Collaboration, Measurement of the fraction of $\Upsilon(1S)$ originating from $\chi_b(1P)$ decays in pp collisions at $\sqrt{s} = 7$ TeV. JHEP **1211**, 031 (2012). [arXiv:1209.0282]
87. S. Chatrchyan et al., CMS Collaboration, Measurement of the $\Upsilon(1S)$, $\Upsilon(2S)$ and $\Upsilon(3S)$ polarizations in pp collisions at $\sqrt{s} = 7$ TeV. Phys. Rev. Lett. **110**, 081802 (2013). [arXiv:1209.2922]

Measurements of the X c and X b Quarkonium States in
pp Collisions with the ATLAS Experiment
Chisholm, A.
2016, XVI, 183 p. 95 illus., 40 illus. in color., Hardcover
ISBN: 978-3-319-23119-8